Compact Ultra Massive Array (CUMA) with 4 RF Chains for Massive Connectivity

Kai-Kit Wong
Department of Electronic and Electrical Engineering (of University College London)
Torrington Place, London, United Kingdom
e-mail: kai-kit.wong@ucl.ac.uk

***Abstract*—The bottleneck for massive connectivity is the need of acquiring accurate channel state information (CSI) from all the users at the transmitter side so that multiuser signals can be nicely placed into orthogonal subspaces for spatial multiplexing. Recently, a transmit CSI-free multiple access technique, referred to as fluid antenna multiple access (FAMA), has been introduced exploiting the unique position reconfigurability of fluid antenna system (FAS). In this paper, we consider one particular version of FAMA, referred to as compact ultra massive array (CUMA). Motivated by the fact that a mobile device operating in the 5G core band has 4 radio-frequency (RF) chains, this paper extends CUMA to exploit all 4 RF chains for improved performance.**

***Index Terms*—Channel state information, compact ultra massive array, fluid antenna system, massive connectivity.**

I. Introduction

EXTREME massive connectivity is one of the most challenging scenarios future-generation wireless communication systems aim to address. In the upcoming sixth-generation (6G), this is equivalent to hitting 1000 bps/Hz [1] which may be interpreted as delivering 1 bps/Hz for 1000 users on the same physical data channel. Under ideal conditions, this is an achievable feat if we have at least 1000 antennas at the base station (BS) and the availability of instantaneous channel state information (CSI) for all 1000 mobile users.[1] In [1], this was envisaged in the cell-free setup where a large number of BSs collaborate to make up the required number of antennas, and precoding was responsible for massive spatial multiplexing.

Nevertheless, the reality of the fifth-generation (5G) mobile networks has given us a shocking lesson. In 5G, instead of the theoretically simple matched filtering precoding in [2], a more complex codebook-based Type II New Radio (NR) multiuser multiple-input multiple-output (MIMO) precoding is employed [3]. It turns out that under practical scenarios, the CSI is not perfect, and the signal-to-interference plus noise ratio (SINR) maximization based precoding in 5G is necessary. Multiuser MIMO perhaps is a more justifiable description than massive MIMO in 5G. Another lesson is that a 5G BS with 64 antennas (and 64 radio-frequency (RF) chains) can only support up to 12 mobile users on the same physical data channel. This once again indicates that the CSI acquisition process over a large number of users is the obstacle. Otherwise, a 64-antenna BS could have easily dealt with 64 users using precoding.

The work of K. K. Wong is supported by the Engineering and Physical Sciences Research Council (EPSRC) under grant EP/W026813/1.

[1]The comment is based on a downlink setup but the same argument follows similarly in the uplink where it is often considered an easier problem because acquiring the CSI from the all users at the BS is a more natural process.

Regarding the cell-free architecture, as a matter of fact, the idea was partially adopted in the fourth-generation (4G) under the name of coordinated multipoint (CoMP) which encouraged BS collaboration for joint signal processing [4]. Also, there has been hopeful discussion of enhancing the CoMP features for 5G [5] but there appears to be a long road ahead if the vision of [6] is to become reality. Besides, it is worth recognizing that precoding is not an upgrade-friendly solution, and any increase in the number of BS antennas as well as precoding capability can only happen after a proper standardization effort.

Facing the limitations of MIMO, there have been efforts in researching other multiple access technologies that can complement multiuser MIMO for enhanced capacity performance. Non-orthogonal multiple access (NOMA) [7]–[9] and rate-splitting multiple access (RSMA) [10] are widely regarded as strong candidates to do so but they share the same difficulty as MIMO of needing CSI at the transmitter side. Additionally, they also require mobile users to adopt successive interference cancellation (SIC). For this reason, they are believed to be only feasible if the number of users is small, e.g., ≤ 3.[2]

Motivated by the above discussion, the emerging concept of fluid antenna multiple access (FAMA) is increasingly attractive [11], [12] because it is CSI-free at the transmitter side. FAMA relies on the antenna position reconfigurability at the receiver to access the spatial opportunity where interference naturally vanishes in deep fade. The idea is very simple and works for any number of mobile users by optimizing the antenna position to where the SINR is maximized in a given space.

Antenna position reconfigurability is captured in the recent concept of fluid antenna system (FAS) that represents all forms of shape-flexible position-flexible antenna technologies [13], [14]. FAS takes advantage of the recent advances in software-defined liquid-based antennas [15], [16], surface wave-based flexible antennas [17], [18], and reconfigurable RF pixel-based antennas [19]–[21]. FAS was first brought to the scene of wireless communications by Wong *et al.* in [22]. Since then, efforts in [23] improved the channel model for a more accurate performance evaluation of FAS while [24], [25] focused on quantifying the diversity order of FAS. Recent results further saw performance analysis of FAS to cope with general fading channels [26], [27]. The results in [28] later revealed that the MIMO-FAS setup where multiple fluid antennas are deployed at both ends could obtain huge diversity gains over the fixed-position MIMO counterpart. Most recent attempts are found to

[2]The majority of work in NOMA and RSMA is limited to 2 to 3 users.

consider continuous antenna position change of FAS [29] and a new block spatial correlation model that offers tractability analysis with accuracy was given in [30]. Besides, application of FAS has been extended to the emerging integrated sensing and communications (ISAC) scenarios [31]. CSI acquisition can be challenging for FAS due to increased dimensionality, which has motivated new estimation methods in [32]–[35]. Overview articles on FAS can be found in [14], [36], [37]. It is noteworthy that the recent efforts under the name of movable antennas fall under the category of FAS, see [38].

While FAS can be viewed as a new degree of freedom (dof) to traditional fixed-antenna systems, multiple access exploiting the unique capability of FAS might be just as exciting. FAMA originally was hypothesized to switch the antenna position at each user on a per-symbol basis [11] but due to its practicality, a slower version of FAMA that only updates the user antenna positions if channels change, was later proposed at the price of reduced multiplexing capability in [12]. The performance of slow FAMA in the two-user case was investigated in [39]. Slow FAMA is nevertheless limited in terms of the number of users that can be handled. Another version of FAMA, referred to as compact ultra massive antenna (CUMA), was therefore proposed in [40]. In CUMA, instead of choosing one 'lucky' position where all the interferers happen to be weak, it turns on a large number of positions with aligned channels to obtain the received signal for detection. This results in an enhanced multiple access capability compared to slow FAMA.

The existing version of CUMA is built on the assumption that there are two RF chains at each mobile receiver. This is a natural setup as CUMA selects the positions (referred to as 'ports') to align the desired user's channel, one set focusing on the real parts and another on the imaginary parts. Each set is superimposed on an RF chain before the two superimposed signals are combined to produce the output signal. However, the fact that the 5G core band currently needs mobile device to have 4 RF chains to operate, suggests that it should be of great interest to see CUMA operate on mobile receivers with 4 RF chains instead. Motivated by this, in this paper, we extend CUMA in [40] to the case with 4 RF chained mobile users and evaluate the performance gain by computer simulations. To simplify our discussion, mutual coupling effects, irrespective of the implementation of FAS, are ignored and we also assume that the wireless channels undergo rich scattering.

II. System Model

A. The FAMA Channel

Our interest is on a multiple access approach that needs no CSI at the transmitter side. Thus, we consider an interference channel where there are U BS transmitters sending independent messages to their respective user equipments (UEs). The BSs are uncoordinated and each BS has a single fixed-antenna for transmission. By contrast, each UE is equipped with a two-dimensional (2D) FAS with size $\bar{W} = W_1\lambda \times W_2\lambda$ where λ is the carrier wavelength. Also, the FAS has $N = N_1 \times N_2$ evenly distributed ports or positions that can be activated to receive the signal. How to decide which ports to be selected

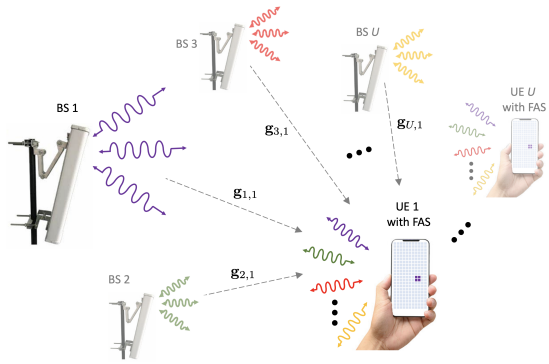

Fig. 1. An interference channel with U single fixed-antenna BS communicating to U UEs each with a 2D FAS.

to be on and how the signals at the activated ports are mixed in CUMA will be explained in Section II-B. In this setup, no joint signal processing between the BSs nor between the UEs is allowed. The overall system model is shown in Fig. 1.

At UE u, the signals that would have been received at the ports when activated can be written in vector form as

$$\mathbf{r}_u = \mathbf{g}_{u,u}s_u + \sum_{\substack{\tilde{u}=1 \\ \tilde{u}\neq u}}^{U} \mathbf{g}_{\tilde{u},u}s_{\tilde{u}} + \boldsymbol{\eta}_u, \tag{1}$$

in which $\mathbf{g}_{\tilde{u},u} \in \mathbb{C}^N$ denotes the complex channels from the $\tilde{u}$-th BS transmitter to the ports of UE u, s_u is the information symbol for UE u with $\mathrm{E}[|s_u^2|] = \sigma_s^2$, and $\boldsymbol{\eta}_u$ denotes the complex additive white Gaussian noise vector at the ports of UE u whose elements are independent, identically distributed (i.i.d.) and have zero mean and variance of σ_η^2. Note that in (1), we have adopted vectorization to convert the supposed 2D channel matrix (e.g., the channels over 2D ports) into a one-dimensional (1D) channel vector, $\mathbf{g}_{\tilde{u},u}$, with an appropriate mapping between the (n_1, n_2)-th port and the k-th port, i.e., $k = \mathrm{map}(n_1, n_2)$. Specifically, we have

$$n_1 = \begin{cases} N_1 \text{ if } k \bmod N_1 = 0, \\ k \bmod N_1 \text{ otherwise}, \end{cases} \tag{2}$$

and

$$n_2 = \begin{cases} \left\lfloor \dfrac{k}{N_1} \right\rfloor \text{ if } n_1 = N_1, \\ \left\lfloor \dfrac{k}{N_1} \right\rfloor + 1 \text{ otherwise}, \end{cases} \tag{3}$$

where $\lfloor x \rfloor$ returns the floor integer of x.

The channel is modelled using the finite scatterer channel model [41] so that

$$\mathbf{g}_{\tilde{u},u} = \sqrt{\frac{K\Omega}{K+1}} e^{j\delta_{\tilde{u},u}} \mathbf{a}(\theta_0^{(\tilde{u},u)}, \phi_0^{(\tilde{u},u)}) + \frac{1}{\sqrt{N_p}} \sqrt{\frac{1}{K+1}} \sum_{\ell=1}^{N_p} \kappa_\ell^{(\tilde{u},u)} \mathbf{a}(\theta_\ell^{(\tilde{u},u)}, \phi_\ell^{(\tilde{u},u)}), \tag{4}$$

in which K is the Rice factor measuring the relative strength of the line-of-sight (LoS) path over the non-LoS paths, $\delta_{\tilde{u},u}$

denotes the phase of the LoS component, $\kappa_\ell^{(\tilde{u},u)}$ represents the complex channel coefficient of the ℓ-th non-LoS component with $\mathrm{E}[\sum_{\forall \ell} |\kappa_\ell^{(\tilde{u},u)}|^2] = \Omega$, N_p is the number of non-LoS paths, and $\mathbf{a}(\theta,\phi)$ is the steering vector given by

$$\mathbf{a}(\theta,\phi) = \left[1 \; e^{j\left(\frac{2\pi W_1}{N_1-1}\right)\sin\theta\cos\phi} \cdots \; e^{j2\pi W_1 \sin\theta\cos\phi}\right]^T \otimes \left[1 \; e^{j\left(\frac{2\pi W_2}{N_2-1}\right)\sin\theta\cos\phi} \cdots \; e^{j2\pi W_2 \sin\theta\cos\phi}\right]^T, \quad (5)$$

where $\otimes$ denotes the Kronecker tensor product, θ and ϕ are, respectively, the azimuth and elevation angle-of-arrival (AoA) of the corresponding path, and the superscript T denotes the transposition operation. The AoAs are uniformly distributed between 0 and 2π and independent. In this model, we have the channel power given by $\Omega = \mathrm{E}[|[\mathbf{g}_{\tilde{u},u}]_k|^2]$ in which $[\cdot]_k$ returns the k-th entry of the input vector. Note that the BSs are assumed to be far apart from each other so that they see completely different sets of scatterers in the environment.

For benchmarking purposes, we define the average signal-to-noise ratio (SNR) as $\Gamma = \frac{\Omega\sigma_s^2}{\sigma_\eta^2}$.

B. Signal Model and Detector for CUMA

The working principle of CUMA is that at each UE, say u, a set of ports, denoted as $\mathcal{K}$, are activated and the received signals at the activated ports are superimposed in the analogue domain without co-phasing. To proceed, we define

$$\begin{cases} r_u^{\mathrm{I}}(\mathcal{K}) = \sum\limits_{k\in\mathcal{K}} \mathrm{real}\left([\mathbf{r}_u]_k\right), \\ r_u^{\mathrm{Q}}(\mathcal{K}) = \sum\limits_{k\in\mathcal{K}} \mathrm{imag}\left([\mathbf{r}_u]_k\right). \end{cases} \quad (6)$$

The above signals correspond to the in-phase and quadrature components of the aggregated complex signal. Denoting the complex information symbol as $s_u = s_u^{\mathrm{I}} + j s_u^{\mathrm{Q}}$, we have

$$r_u^{\mathrm{I}}(\mathcal{K}) = \left[\sum_{k\in\mathcal{K}} \mathrm{real}\left([\mathbf{g}_{u,u}]_k\right)\right] s_u^{\mathrm{I}} + \left[-\sum_{k\in\mathcal{K}} \mathrm{imag}\left([\mathbf{g}_{u,u}]_k\right)\right] s_u^{\mathrm{Q}} + \sum_{k\in\mathcal{K}} \mathrm{real}\left(\left[\sum_{\substack{\tilde{u}=1\\ \tilde{u}\neq u}}^{U} \mathbf{g}_{\tilde{u},u} s_{\tilde{u}} + \boldsymbol{\eta}_u\right]_k\right) \quad (7)$$

and

$$r_u^{\mathrm{Q}}(\mathcal{K}) = \left[\sum_{k\in\mathcal{K}} \mathrm{imag}\left([\mathbf{g}_{u,u}]_k\right)\right] s_u^{\mathrm{I}} + \left[\sum_{k\in\mathcal{K}} \mathrm{real}\left([\mathbf{g}_{u,u}]_k\right)\right] s_u^{\mathrm{Q}} + \sum_{k\in\mathcal{K}} \mathrm{imag}\left(\left[\sum_{\substack{\tilde{u}=1\\ \tilde{u}\neq u}}^{U} \mathbf{g}_{\tilde{u},u} s_{\tilde{u}} + \boldsymbol{\eta}_u\right]_k\right). \quad (8)$$

In order to obtain the real-valued signals $r_u^{\mathrm{I}}(\mathcal{K})$ and $r_u^{\mathrm{Q}}(\mathcal{K})$, UE u simply retrieves the in-phase and quadrature components of the superposition of the received signals from the activated ports, according to some set $\mathcal{K}$. No scaling nor phase shifting is required before aggregation, so only one RF chain suffices to obtain the two real-valued output signals.

In [40], it was proposed to obtain two sets, $\mathcal{K}_1$ and $\mathcal{K}_2$. One attempts to select the ports where the real parts of the desired user channels are aligned (i.e., all positive or all negative), while another set does the same but focusing on the imaginary parts of the desired user channels. If we now denote the set that contains the ports that have all positive in-phase channels for the desired user channel as $\mathcal{K}_1^+$ and all negative in-phase channels as $\mathcal{K}_1^-$, then $\mathcal{K}_1$ can be determined by deciding on whether all positive in-phase or all negative in-phase channels are preferred. In particular, this can be done by

$$\left|\sum_{k\in\mathcal{K}_1^+} \mathrm{real}\left([\mathbf{g}_{u,u}]_k\right)\right| \underset{\mathcal{K}_1^-}{\overset{\mathcal{K}_1^+}{\gtrless}} \left|\sum_{k\in\mathcal{K}_1^-} \mathrm{real}\left([\mathbf{g}_{u,u}]_k\right)\right|. \quad (9)$$

The set $\mathcal{K}_1$ chooses between $\mathcal{K}_1^+$ and $\mathcal{K}_1^-$ according to (9). Similarly, we also have the set $\mathcal{K}_2$ such that

$$\left|\sum_{k\in\mathcal{K}_2^+} \mathrm{imag}\left([\mathbf{g}_{u,u}]_k\right)\right| \underset{\mathcal{K}_2^-}{\overset{\mathcal{K}_2^+}{\gtrless}} \left|\sum_{k\in\mathcal{K}_2^-} \mathrm{imag}\left([\mathbf{g}_{u,u}]_k\right)\right|, \quad (10)$$

where $\mathcal{K}_2^+$ and $\mathcal{K}_2^-$ are defined similarly.

With $\mathcal{K}_1$ and $\mathcal{K}_2$, known, UE u can estimate its symbol by

$$\tilde{\boldsymbol{s}}_u = \begin{bmatrix} A & -a \\ a & A \\ b & -B \\ B & b \end{bmatrix}^{-1} \begin{bmatrix} r_u^{\mathrm{I}}(\mathcal{K}_1) \\ r_u^{\mathrm{Q}}(\mathcal{K}_1) \\ r_u^{\mathrm{I}}(\mathcal{K}_2) \\ r_u^{\mathrm{Q}}(\mathcal{K}_2) \end{bmatrix}, \quad (11)$$

where

$$\begin{cases} A = \sum\limits_{k\in\mathcal{K}_1} \mathrm{real}\left([\mathbf{g}_{u,u}]_k\right), \quad a = \sum\limits_{k\in\mathcal{K}_1} \mathrm{imag}\left([\mathbf{g}_{u,u}]_k\right), \\ B = \sum\limits_{k\in\mathcal{K}_2} \mathrm{imag}\left([\mathbf{g}_{u,u}]_k\right), \; b = \sum\limits_{k\in\mathcal{K}_2} \mathrm{real}\left([\mathbf{g}_{u,u}]_k\right). \end{cases} \quad (12)$$

III. Extension to 4 RF Chains

The standard version of CUMA as proposed in [40] assumes that there are only two RF chains at each UE receiver. If there are now 4 RF chains available, then instead of having only two sets, $\mathcal{K}_1$ and $\mathcal{K}_2$, we can have up to four sets and combine the signals from them to improve detection performance. Also, the comparison in (9) and (10) becomes unnecessary. Hence,

$$\tilde{\boldsymbol{s}}_u = \begin{bmatrix} A & -a \\ a & A \\ C & -c \\ c & C \\ b & -B \\ B & b \\ d & -D \\ D & d \end{bmatrix}^{-1} \begin{bmatrix} r_u^{\mathrm{I}}(\mathcal{K}_1^+) \\ r_u^{\mathrm{Q}}(\mathcal{K}_1^+) \\ r_u^{\mathrm{I}}(\mathcal{K}_1^-) \\ r_u^{\mathrm{Q}}(\mathcal{K}_1^-) \\ r_u^{\mathrm{I}}(\mathcal{K}_2^+) \\ r_u^{\mathrm{Q}}(\mathcal{K}_2^+) \\ r_u^{\mathrm{I}}(\mathcal{K}_2^-) \\ r_u^{\mathrm{Q}}(\mathcal{K}_2^-) \end{bmatrix}, \quad (13)$$

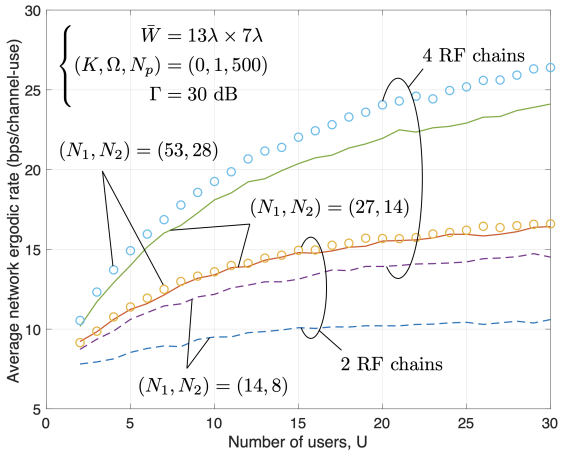

Fig. 2. Rate performance against the number of users.

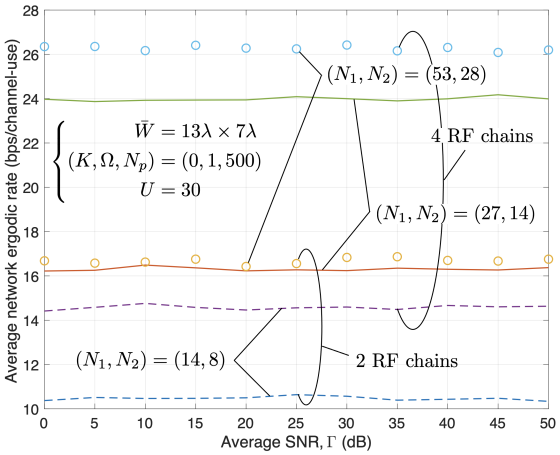

Fig. 3. Rate performance against the SNR.

where

$$\begin{cases} A = \sum\limits_{k \in \mathcal{K}_1^+} \text{real}\left([\mathbf{g}_{u,u}]_k\right), \quad a = \sum\limits_{k \in \mathcal{K}_1^+} \text{imag}\left([\mathbf{g}_{u,u}]_k\right), \\ C = \sum\limits_{k \in \mathcal{K}_1^-} \text{real}\left([\mathbf{g}_{u,u}]_k\right), \quad c = \sum\limits_{k \in \mathcal{K}_1^-} \text{imag}\left([\mathbf{g}_{u,u}]_k\right), \\ B = \sum\limits_{k \in \mathcal{K}_2^+} \text{imag}\left([\mathbf{g}_{u,u}]_k\right), \; b = \sum\limits_{k \in \mathcal{K}_2^+} \text{real}\left([\mathbf{g}_{u,u}]_k\right), \\ D = \sum\limits_{k \in \mathcal{K}_2^-} \text{imag}\left([\mathbf{g}_{u,u}]_k\right), \; d = \sum\limits_{k \in \mathcal{K}_2^-} \text{real}\left([\mathbf{g}_{u,u}]_k\right). \end{cases} \tag{14}$$

IV. Simulation Results

In this section, we evaluate the rate performance of CUMA with an increased number of RF chains at each mobile UEs using Monte Carlo simulations. The parameters $(\rho, N_{\max}) = (0.4, 240)$ have been set and for definitions of these parameters in CUMA, readers are referred to [40]. The results could be interpreted as having the carrier frequency of 26 GHz, and each FAS size as $15\ \text{cm} \times 8\ \text{cm}$ if $\bar{W} = 13\lambda \times 7\lambda$. In the simulations, we considered rich scattering so that $N_p = 500$ with or without the LoS. We note that at such frequency, the channel does not normally have rich scattering phenomenon but it can be easily restored by using a large number of random scattering surfaces [42]. In the figures, other related system parameters are clearly stated when needed.

Fig. 2 provides the average network rate results against the number of users in the system. As we can see, the network rate increases with the number of users despite a diminishing return. This illustrates that CUMA can effectively deal with multiple access even though no precoding is used at the BS and no SIC is adopted at the UEs. The results also show that having 4 RF chains instead of 2 gives a significant boost in rate performance and the performance gain by increasing the number of ports is also more apparent. The results in Fig. 3 however indicate that the rate performance is invariant over a wide range of SNR, which is expected in the interference-limited regime. The great performance of CUMA also does not depend on whether the LoS is present, as shown in Fig. 4. Finally, Fig. 5 reveals that

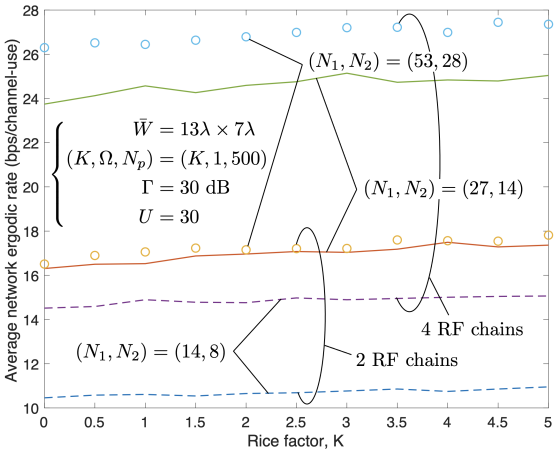

Fig. 4. Rate performance against the Rice factor.

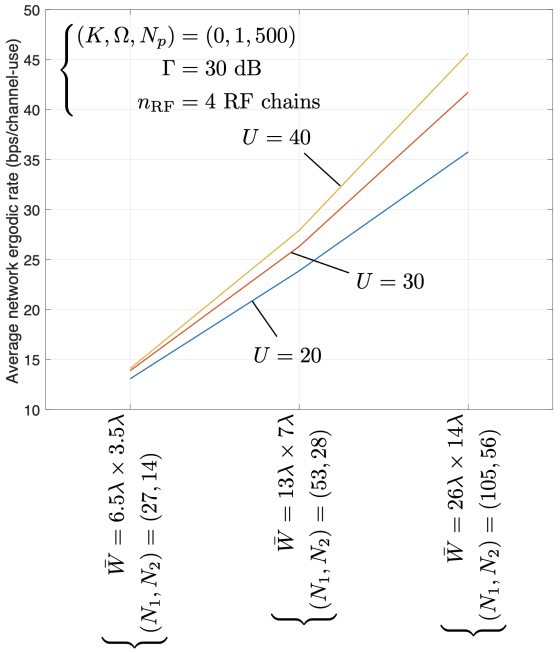

Fig. 5. Rate performance against the size of FAS.

the size of FAS at each UE plays a major role in the rate performance, as expected.

V. Conclusion

In this paper, we has extended CUMA, a recently developed multiple access scheme using FAS, to the case where each UE has 4 RF chains. The simulation results demonstrated that the rate performance of CUMA can be significantly enhanced.

References

[1] X. You *et al.*, "Toward 6G TKμ extreme connectivity: Architecture, key technologies and experiments," *IEEE Wireless Commun.*, vol. 30, no. 3, pp. 86–95, Jun. 2023.

[2] T. L. Marzetta, "Noncooperative cellular wireless with unlimited numbers of base station antennas," *IEEE Trans. Wireless Commun.*, vol. 9, no. 11, pp. 3590–3600, Nov. 2010.

[3] D. A. Urquiza Villalonga, H. OdetAlla, M. J. Fernández-Getino Garca, and A. Flizikowski, "Spectral efficiency of precoded 5G-NR in single and multi-user scenarios under imperfect channel knowledge: A comprehensive guide for implementation," *Electronics*, vol. 11, no. 24, p. 4237, Dec. 2022.

[4] R. Irmer *et al.*, "Coordinated multipoint: Concepts, performance, and field trial results," *IEEE Commun. Mag.*, vol. 49, no. 2, pp. 102–111, Feb. 2011.

[5] Q. Cui *et al.*, "Evolution of limited-feedback CoMP systems from 4G to 5G: CoMP features and limited-feedback approaches," *IEEE Veh. Technol. Mag.*, vol. 9, no. 3, pp. 94–103, Sept. 2014.

[6] H. Q. Ngo, A. Ashikhmin, H. Yang, E. G. Larsson, and T. L. Marzetta, "Cell-free massive MIMO versus small cells," *IEEE Trans. Wireless Commun.*, vol. 16, no. 3, pp. 1834–1850, Mar. 2017.

[7] Z. Ding *et al.*, "A survey on non-orthogonal multiple access for 5G networks: Research challenges and future trends," *IEEE J. Select. Areas Commun.*, vol. 35, no. 10, pp. 2181–2195, Oct. 2017.

[8] Y. Liu *et al.*, "Evolution of NOMA toward next generation multiple access (NGMA) for 6G," *IEEE J. Select. Areas Commun.*, vol. 40, no. 4, pp. 1037–1071, Apr. 2022.

[9] Y. Liu *et al.*, "Developing NOMA to next generation multiple access: Future vision and research opportunities," *IEEE Wireless Commun.*, vol. 29, no. 6, pp. 120–127, Dec. 2022.

[10] B. Clerckx *et al.*, "A primer on rate-splitting multiple access: Tutorial, myths, and frequently asked questions," *IEEE J. Select. Areas Commun.*, vol. 41, no. 5, pp. 1265–1308, May 2023.

[11] K. K. Wong, and K. F. Tong, "Fluid antenna multiple access," *IEEE Trans. Wireless Commun.*, vol. 21, no. 7, pp. 4801–4815, Jul. 2022.

[12] K. K. Wong, D. Morales-Jimenez, K.-F. Tong, and C.-B. Chae, "Slow fluid antenna multiple access," *IEEE Trans. Commun.*, vol. 71, no. 5, pp. 2831–2846, May 2023.

[13] K.-K. Wong, K.-F. Tong, Y. Zhang, and Z. Zheng, "Fluid antenna system for 6G: When Bruce Lee inspires wireless communications," *Elect. Lett.*, vol. 56, no. 24, pp. 1288–1290, Nov. 2020.

[14] K. K. Wong, K.-F. Tong, Y. Shen, Y. Chen, and Y. Zhang, "Bruce Lee-inspired fluid antenna system: Six research topics and the potentials for 6G," *Frontiers Commun. Netw.*, vol. 3, no. 853416, Mar. 2022.

[15] Y. Huang, L. Xing, C. Song, S. Wang, and F. Elhouni, "Liquid antennas: Past, present and future," *IEEE Open J. Antennas & Propag.*, vol. 2, pp. 473–487, Mar. 2021.

[16] C. Borda-Fortuny, L. Cai, K. F. Tong, and K. K. Wong, "Low-cost 3D-printed coupling-fed frequency agile fluidic monopole antenna system," *IEEE Access*, vol. 7, pp. 95058–95064, Jul. 2019.

[17] Y. Shen, K.-F. Tong, and K. K. Wong, "Radiation pattern diversified double-fluid-channel surface-wave antenna for mobile communications," in *Proc. IEEE-APS Topical Conf. Antennas & Propag. Wireless Commun. (APWC)*, pp. 085–088, 5-9 Sept. 2022, Cape Town, South Africa.

[18] H. Wang, Y. Shen, K.-F. Tong, and K. K. Wong, "Continuous electrowetting surface-wave fluid antenna for mobile communications," in *Proc. IEEE Region 10 Conference (TENCON)*, 1-4 Nov. 2022, Hong Kong.

[19] B. A. Cetiner *et al.*, "Multifunctional reconfigurable MEMS integrated antennas for adaptive MIMO systems," *IEEE Commun. Mag.*, vol. 42, no. 12, pp. 62–70, Dec. 2004.

[20] A. Grau Besoli, and F. De Flaviis, "A multifunctional reconfigurable pixeled antenna using MEMS technology on printed circuit board," *IEEE Trans. Antennas & Propag.*, vol. 59, no. 12, pp. 4413–4424, Dec. 2011.

[21] L. Jing, M. Li, and R. Murch, "Compact pattern reconfigurable pixel antenna with diagonal pixel connections," *IEEE Trans. Antennas & Propag.*, vol. 70, no. 10, pp. 8951–8961, Oct. 2022.

[22] K. K. Wong, A. Shojaeifard, K.-F. Tong, and Y. Zhang, "Fluid antenna systems," *IEEE Trans. Wireless Commun.*, vol. 20, no. 3, pp. 1950–1962, Mar. 2021.

[23] M. Khammassi, A. Kammoun, and M.-S. Alouini, "A new analytical approximation of the fluid antenna system channel," *IEEE Trans. Wireless Commun.*, vol. 22, no. 12, pp. 8843–8858, Dec. 2023.

[24] W. K. New, K.-K. Wong, H. Xu, K.-F. Tong, and C.-B. Chae, "Fluid antenna system: New insights on outage probability and diversity gain," *IEEE Trans. Wireless Commun.*, vol. 23, no. 1, pp. 128–140, Jan. 2024.

[25] J. D. Vega-Sánchez, A. E. López-Ramírez, L. Urquiza-Aguiar and D. P. M. Osorio, "Novel expressions for the outage probability and diversity gains in fluid antenna system," *IEEE Wireless Commun. Lett.*, early access, doi: 10.1109/LWC.2023.3329780.

[26] P. D. Alvim *et al.*, "On the performance of fluid antennas systems under α-μ fading channels," *IEEE Wireless Commun. Lett.*, early access, doi: 10.1109/LWC.2023.3322106.

[27] F. R. Ghadi, K.-K. Wong, F. J. López-Martínez, and K.-F. Tong, "Copula-based performance analysis for fluid antenna systems under arbitrary fading channels," *IEEE Commun. Lett.*, vol. 27, no. 11, pp. 3068–3072, Nov. 2023.

[28] W. K. New, K.-K. Wong, H. Xu, K.-F. Tong, and C.-B. Chae, "An information-theoretic characterization of MIMO-FAS: Optimization, diversity-multiplexing tradeoff and q-outage capacity," *IEEE Trans. Wireless Commun.*, early access, doi:10.1109/TWC.2023.3327063, 2024.

[29] C. Psomas, P. J. Smith, H. A. Suraweera and I. Krikidis, "Continuous fluid antenna systems: Modeling and analysis," *IEEE Commun. Lett.*, vol. 27, no. 12, pp. 3370–3374, Dec. 2023.

[30] P. Ramirez-Espinosa, D. Morales-Jimenez, and K.-K. Wong, "A new spatial block-correlation model for fluid antenna systems," *arXiv preprint*, arXiv:2401.04513, 2024.

[31] C. Wang *et al.*, "Fluid antenna system liberating multiuser MIMO for ISAC via deep reinforcement learning," *IEEE Trans. Wireless Commun.*, early access, doi:10.1109/TWC.2024.3376800, 2024.

[32] C. Skouroumounis and I. Krikidis, "Fluid antenna with linear MMSE channel estimation for large-scale cellular networks," *IEEE Trans. Commun.*, vol. 71, no. 2, pp. 1112–1125, Feb. 2023.

[33] H. Xu *et al.*, "Channel estimation for FAS-assisted multiuser mmWave systems," accepted in *IEEE Commun. Lett.*, 2024.

[34] Z. Zhang, J. Zhu, L. Dai, and R. W. Heath Jr, "Successive Bayesian reconstructor for channel estimation in fluid antenna systems," *arXiv preprint*, arXiv:2312.06551v3, Jan. 2024.

[35] J. Zou, S. Sun and C. Wang, "Online learning-induced port selection for fluid antenna in dynamic channel environment," *IEEE Wireless Commun. Lett.*, early access, doi: 10.1109/LWC.2023.3328420.

[36] K.-K. Wong, W. K. New, X. Hao, K.-F. Tong, and C.-B. Chae, "Fluid antenna system—Part I: Preliminaries," *IEEE Commun. Lett.*, vol. 27, no. 8, pp. 1919–1923, Aug. 2023.

[37] J. Zheng *et al.*, "Flexible-position MIMO for wireless communications: Fundamentals, challenges, and future directions," arXiv preprint, arXiv:2308.14578 [cs.IT], Nov. 2023.

[38] L. Zhu and K. K. Wong, "Historical review of fluid antenna and movable antenna," *arXiv preprint*, arXiv:2401.02362v2, 2024.

[39] H. Xu *et al.*, "Revisiting outage probability analysis for two-user fluid antenna multiple access system," *IEEE Trans. Wireless Commun.*, early access, doi:10.1109/TWC.2024.3363499, 2024.

[40] K.-K. Wong, C.-B. Chae, and K.-F. Tong, "Compact ultra massive antenna array: A simple open-loop massive connectivity scheme," *IEEE Trans. Wireless Commun.*, early access, doi:10.1109/TWC.2023.3330932, 2023.

[41] T. S. Rappaport, G. R. MacCartney, M. K. Samimi, and S. Sun, "Wide-band millimeter-wave propagation measurements and channel models for future wireless communication system design," *IEEE Trans. Commun.*, vol. 63, no. 9, pp. 3029–3056, 2015.

[42] K. K. Wong, K. F. Tong, and C. B. Chae, "Fluid antenna system—Part III: A new paradigm of distributed artificial scattering surfaces for massive connectivity," *IEEE Commun. Lett.*, vol. 27, no. 8, pp. 1929–1933, Aug. 2023.